

Extracting polygonal footprints in off-nadir images with Segment Anything Model

Kai Li^{a,b,c}, Jingbo Chen^a, Yupeng Deng^a, Yu Meng^{a,*}, Diyou Liu^a, Junxian Ma^{a,c}, Chenhao Wang^{a,c},
Xiangyu Zhao^b

^a*Aerospace Information Research Institute, Chinese Academy of Sciences, Beijing 100101, China*

^b*School of Data Science, City University of Hong Kong, Hong Kong 999077, China*

^c*School of Electronic Electrical and Communication Engineering, University of Chinese Academy of Sciences, Beijing 100049, China*

Abstract

Building Footprint Extraction (BFE) from off-nadir aerial images often involves roof segmentation and offset prediction to adjust roof boundaries to the building footprint. However, this multi-stage approach typically produces low-quality results, limiting its applicability in real-world data production. To address this issue, we present OBMv2, an end-to-end and promptable model for polygonal footprint prediction. Unlike its predecessor OBM, OBMv2 introduces a novel Self Offset Attention (SOFA) mechanism that improves performance across diverse building types, from bungalows to skyscrapers, enabling end-to-end footprint prediction without post-processing. Additionally, we propose a Multi-level Information System (MISS) to effectively leverage roof masks, building masks, and offsets for accurate footprint prediction. We evaluate OBMv2 on the BONAI and OmniCity-view3 datasets and demonstrate its generalization on the Huizhou test set. The code will be available at <https://github.com/likaiucas/OBMv2>.

Keywords: Building footprint extraction, building detection, Segment Anything Model (SAM), Offset-Building Model (OBM), off-nadir aerial image, Nadaraya-Watson regression, look-ahead masking

1. Introduction

Building Footprint Extraction (BFE) has been a subject of research for over a decade, forming the foundation for critical tasks such as 3D building reconstruction and building change detection. Early approaches to BFE primarily employed machine learning algorithms (Inglada, 2007) and geometric features (Lafarge et al., 2010; Ortner et al., 2008). However, these techniques were often hindered by their reliance on shallow features, manual measurements, and limited generalization, creating a demand for more sophisticated methodologies.

The rise of deep convolutional networks revolutionized BFE, with offset-based methods gaining popularity as a reliable and cost-efficient solution (Christie

et al., 2020; Li et al., 2021; Wang et al., 2023a; Li et al., 2024c,a). Offset-based techniques are particularly well-suited for processing off-nadir images, which can be easily captured by satellite cameras at varying angles, making them more affordable and offering greater spatial coverage compared to LiDAR-based approaches (Priestnall et al., 2000; Khattak et al., 2013; Kunwar et al., 2021; Lian et al., 2021). This flexibility and cost efficiency have made offset-based methods a preferred choice for solving the BFE problem.

Despite the advancements in offset-based methods, several limitations persist. Christie et al. (2020) introduced a technique that employs a U-Net decoder with a ResNet encoder to predict both image-level orientations and per-pixel height values. This method derives final flow offsets by multiplying the orientation and pixel-level height values. However, it is primarily focused on single-task height estimation and requires demanding training prerequisites.

To address these limitations, Li et al. (2021) proposed a multi-task learning model known as MTBR-

*Yu Meng is the corresponding author.

This research was funded by the National Key R&D Program of China under Grant number 2021YFB3900504.

Here is information on the communication with Kai Li, which will be interact with the journal editors. likai211@mails.ucas.ac.cn

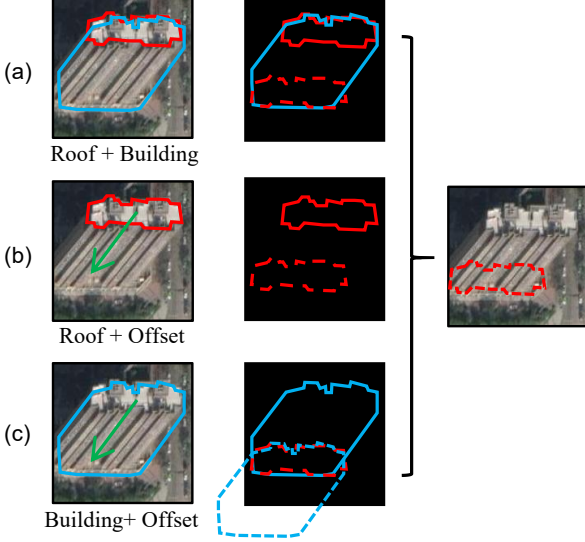


Figure 1: This figure illustrates how to search building footprints with limited information. In (a), with roof segmentation and building segmentation, we find a path on the building map via which the roof can find a place better fitting the footprint. In (b), the building footprint was derived by dragging the roof via the offset. In (c), dragging building segmentation via the offset and the union of both masks represents the building footprint. If building segmentation moves in the opposite direction, the union can represent the roof segmentation.

Net, which enhances the learning process by incorporating an image-wise offset angle prediction task, two pixel-wise offset field prediction tasks, and several semantic-related tasks. In 2023, Wang et al. (2023a) developed an instance-level model called LOFT, based on Mask R-CNN (He et al., 2017), which streamlined the multi-task training labels. LOFT employs an offset Region of Interest (ROI) head to extract roof-to-footprint offsets for each instance building identified by the Region Proposal Network (RPN). The final footprint masks are generated by aligning the predicted roofs to their corresponding footprints using these offsets. Nevertheless, the cost of annotating remote sensing images with offsets remains high, limiting the training diversity.

To further this effort, Li et al. (2024c) introduced the Multi-Level Supervised Building Reconstruction Network (MLS-BRN), building upon LOFT by adding four additional tasks: (1) off-nadir angle prediction; (2) offset angle prediction; (3) footprint segmentation; and (4) real-world height prediction.

Despite these advancements, ROI-based methods often face challenges in practical applications due to the instability of the Region Proposal Network (RPN) and Non-Maximum Suppression (NMS) algorithms

(Viola and Jones, 2001). To address these issues, Li et al. (2024a) introduced OBM, which is based on the architecture of the Segment Anything Model (SAM) (Kirillov et al., 2023). OBM is a promptable model fully constructed with Transformers. It predicts prompt-level offsets through the Reference Offset Augmentation Module (ROAM) using the concept of offset queries. During prompt-level testing, a significant performance disparity was observed between predicting longer and shorter offsets. Additionally, Distance NMS algorithms were developed to tackle this challenge.

At this juncture, it appeared that the BFE problem was nearing resolution. Our next objective was to enhance the quality of the output masks, similar to the advancements seen with SAM-HQ in general computer vision (Ke et al., 2024). However, the effectiveness of these more intuitive experiments has yet to be substantiated by our results. To ensure that the model outputs align more closely with production data, which typically features clear vectorized boundaries and vertices, we propose OBMv2 in this paper.

OBMv2 is a versatile model that supports both prompting and end-to-end approaches, offering both mask and polygonal results. It includes an additional segmentation task to generate a building vertex map for each prompt. To optimize this task’s training, we introduce a new loss function, Dynamic Scope Binary Cross Entropy Loss (DS-BCE Loss), which mitigates the grid effect in output results. The offset prediction pattern identified by Li et al. (2024a) is further refined with a Self Offset Attention (SOFA) layer, specifically designed for offsets. SOFA is formulated using Nadaraya-Watson Regression (Nadaraya, 1964; Watson, 1964). This enables OBMv2 to directly predict footprint vertices without relying on post-processing algorithms like DNMS and NMS. The SOFA module can be effectively employed in both end-to-end and prompting models.

Moreover, traditional "roof-to-footprint" methods, such as OBM and LOFT, depend heavily on the accuracy of roof mask predictions. However, the BFE problem can be intuitively framed as involving building segmentation, roof segmentation, offset prediction, and facade segmentation, as illustrated in Fig.1. This perspective is inspired by The Law of Geography (Zhu et al., 2018), which posits that information in spatial representation is often redundant. The proposed MISS system in this paper broadens the input

types for addressing BFE challenges, thereby diversifying problem-solving methodologies.

Furthermore, OBMv2 facilitates automatic building footprint extraction through mask prompting. A proposal network generates these mask prompts. Notably, OBMv2 features a semantic segmentation head constructed entirely with a pure transformer structure, which serves as the default setting for generating auto prompts. In experimental settings, OBMv2 was integrated with other building-related models, excluding the semantic head.

In summary, the contributions of this paper are as follows:

- OBMv2 can extract polygonal building footprints in both prompting and automatic modes. In contrast to previous methods, it directly predicts footprint polygons, facilitating end-to-end extraction. OBMv2 introduces a novel concept of vertex tokens for obtaining polygonal results, alongside the Dynamic Scope Binary Cross Entropy Loss (DS-BCE Loss) specifically designed for vertex tasks. This makes OBMv2 the first model to predict polygonal footprint results directly through vector operations.
- We propose the Self Offset Attention (SOFA) module to enhance offset prediction. This layer is applicable to other offset-based models, such as LOFT. The SOFA block is a learnable component designed based on interpretable real-world features, demonstrating a successful integration of remote sensing expertise with machine learning techniques.
- We explore the multiplicity of solutions for BFE problems by utilizing spatial correlation. By integrating OBMv2 with other building-related methods, the model can automatically extract building footprints. This multi-solution approach to the BFE problem, proposed for the first time, opens avenues for exploring diverse forms of problem decomposition at the prompt level.

2. Related work

OBMv2 is a multi-task network built upon the architecture of the Segment Anything Model (SAM) (Kirillov et al., 2023), integrating tasks such as prompt segmentation, polygon extraction, and offset learning. The Self Offset Attention (SOFA) block is de-

signed using the Nadaraya-Watson regression framework and an attention mechanism. This paper also explores the multiplicity of solutions for BFE by leveraging existing geometric relationships, geographical knowledge, and iterative methods to enhance performance.

In the following subsections, we will review related works in the application of SAM, polygonal building extraction, and building offset methods to highlight the novelty and contributions of OBMv2.

2.1. Segment Anything Model and its Application

The Segment Anything Model (SAM) (Kirillov et al., 2023) is a foundational model for segmentation, supporting tasks using point, bounding box, and semantic prompts. Ravi et al. (2024) introduced SAM 2 for promptable image and video segmentation, offering faster inference speeds and improved accuracy on both image and video tasks compared to the original SAM. Point to Prompt (P2P) (Guo et al., 2024), also based on SAM, transforms point supervision into fine visual prompts through a two-stage iterative refinement process. Additionally, GaussianVTON (Chen et al., 2024b) employed a SAM-based model for post-editing view images after face refinement. SAM-HQ (Ke et al., 2024) enhanced the quality of SAM’s image embeddings by incorporating deconvolution blocks, while OBM (Li et al., 2024a) introduced offset tokens and the ROAM structure to enable SAM to extract footprint masks.

In this paper, OBMv2 builds upon the idea of SAM-HQ to generate high-quality semantic prompts for automatic extraction. Furthermore, OBMv2 introduces a novel concept of vertex tokens to accurately extract roof key points.

2.2. Polygonal mapping of buildings

Polygonal mapping of buildings involves extracting vectorized building instances that accurately represent building edges. Douglas and Peucker (1973) introduced the Douglas-Peucker simplification techniques, but these algorithms often produce rough results that fail to capture the high-quality edges of buildings. Wei et al. (2019) proposed refinement strategies based on empirical building shapes, while Girard et al. (2021) used Frame-Field methods to better align extracted fields with ground truth contours. Zorzi et al. (2021) described all building polygons in an image as an undirected graph, connecting detected vertices to form the building boundaries. Hisup (Xu

et al., 2023) addressed the challenge of mask reversibility by using deep convolutional neural networks for vertex extraction, followed by boundary tracing of predicted building segmentations to connect the vertices.

In this paper, OBMv2 introduces the concept of vertex tokens for extracting vertices, and these vertices are connected using a strategy similar to Hisup. Unlike the aforementioned methods, OBMv2 is the first model capable of extracting polygonal building footprints from off-nadir images. The footprint polygons are derived through vector operations, offering higher precision.

2.3. Offset-based footprint extraction

Extracting building footprints through offset-based methods leverages the structural similarity between roofs and footprints. Christie et al. (2020) proposed a method using a U-Net decoder to predict image-level orientation and pixel-level height values. Building upon this, Li et al. (2021, 2024c) introduced multi-task learning approaches for the BFE problem, enabling models to train on datasets with varying labels. LOFT (Wang et al., 2023a) was later developed to extract building footprints as part of an instance segmentation task, representing a building footprint with a roof mask and roof-to-footprint offset. OBM (Li et al., 2024a) was the first model to tokenize offset representations and extract building footprints using SAM.

In this paper, we expand on traditional offset-based methods, solving the BFE problem by integrating multiple tasks rather than relying solely on offsets. Prior knowledge is applied to explore the potential of using various sources of information. For instance, we investigate how building footprints can be extracted through a combination of building segmentation and offsets, or through building and roof segmentation. Finally, OBMv2 is integrated with other models to enable fully automatic building footprint extraction.

3. Methodology

This section outlines the methodology of this study. We begin by reintroducing the Building Footprint Extraction (BFE) problem, followed by a detailed explanation of the modifications introduced in OBMv2 compared to OBM. Additionally, we will present the Self Offset Attention (SOFA) and the Multi-Information Spatial Segmentation (MISS) modules in separate sections.

3.1. Problem Statement

In an off-nadir remote sensing image I , there are N buildings represented as $\hat{B} = \hat{b}_1, \hat{b}_2, \dots, \hat{b}_N$. The BFE problem is defined as identifying the building footprints $F = f_1, f_2, \dots, f_N$. In OBM, each building \hat{b}_i is represented by a corresponding prompt p_i , which is interactively fed into the model along with the image I . The model then predicts the roof segmentation r_i and the roof-to-footprint offset o_i . The footprint f_i is derived by applying the offset to the roof mask in the evaluation stage.

In OBMv2, the process is enhanced with the capability for fully automatic footprint prediction, allowing p_i to be empty. OBMv2 introduces a roof vertex segmentation task to extract vertex points v_i for each building \hat{b}_i , and re-focuses on body segmentation b_i as part of the MISS framework. Additionally, in OBMv2, prompts are primarily designed for roof-related tasks, differing from OBM by reducing semantic overlap in off-nadir scenarios.

In summary, OBMv2 introduces two additional prompt-level segmentation tasks along with a global semantic segmentation task for prompting: (1) prompt-level roof vertex segmentation task; (2) prompt-level building segmentation; (3) roof semantic segmentation.

3.2. Self Offset Attention (SOFA)

In prior experiments by Li et al. (2024a), it was observed that models in prompt mode performed better when extracting footprints of taller buildings with significant offsets compared to lower buildings. To address this, Li et al. (2024a) introduced DNMS and soft DNMS as post-processing techniques for correcting offsets. These methods relied on OpenCV operators¹ to process roof masks and offsets to derive the final building footprints.

In this paper, we propose a novel, trainable Self Offset Attention (SOFA) mechanism based on Nadaraya-Watson Regression (Nadaraya, 1964; Watson, 1964) and Look-Ahead Masking (Vaswani et al., 2017) techniques used in Natural Language Processing (NLP). The SOFA module is designed to address the performance disparity seen in buildings with different offset lengths. The diagram for SOFA is presented in Fig. 2.

In machine learning, attention layers can be interpreted as pooling mechanisms. The key role of

¹<https://github.com/opencv/opencv>

for those shorter offsets. Finally, angle-level SOFA can be expressed as:

$$\begin{aligned}\dot{\alpha} &= SOFA_a(\rho, \alpha) \\ &= \sum_{i=1}^n \text{softmax} \left(-\frac{1}{2} (w \times \mathcal{M}(\rho - \rho_i))^2 \right) \alpha_i\end{aligned}\quad (6)$$

Based on similar mathematical reasoning processes, vector-level SOFA can be written as:

$$\begin{aligned}\dot{\vec{o}} &= SOFA_v(\rho, \vec{u}_i) \\ &= \rho \sum_{i=1}^n \text{softmax} \left(-\frac{1}{2} (w \times \mathcal{M}(\rho - \rho_i))^2 \right) \vec{u}_i\end{aligned}\quad (7)$$

\vec{u}_i is the unit offset. $\dot{\vec{o}}$ is the output offset.

The w among the mentioned operation was set to 0. Based on our experiment, this parameter fluctuated at around 0 while training.

From Eq.6 and Eq.7, SOFA is a portable and plug-and-play block, because (1) the learnable parameter w was light; (2) in one off-nadir image I , the number of buildings N tends to be under 100, making the matrix’s spatial operation not consume much GPU memory.

3.3. Network Structure

Fig.2 (a) illustrates the architecture of the proposed Offset Building Model v2 (OBMv2), which introduces four key advancements over OBM.

First, the Self Offset Attention (SOFA) block is inserted between the Feed-Forward Network (FFN) and the Offset Coder ROAM structure. The SOFA block plays a pivotal role in OBMv2 by providing global awareness for each offset head and encoded offset, enabling shorter offsets to minimize error more effectively and enhancing the model’s overall accuracy.

Second, prompt-level vertex segmentation is incorporated into the decoder through the addition of a vertex token. This feature integrates with the HiSup method (Xu et al., 2023) to extract polygonal building footprints.

Third, one of the standout features of OBMv2 is its ability to receive automatic prompts from other models via a Proposal Network, which highlights the model’s efficiency and adaptability.

Lastly, OBMv2 uses roof-related information as prompts to reduce the overlap between buildings, im-

proving the model’s ability to differentiate between them.

To clarify the network structure, it is broken down into three components: Extracting Polygonal Footprints, Proposal Network and Network Setting.

3.3.1. Extracting Polygonal Footprints

The original OBM lacked the ability to extract polygonal footprints. OBMv2 addresses this limitation by utilizing a roof and vertex segmentation task. The overall data flow is illustrated in Fig.2 (a).

First, a new vertex token is initialized alongside mask and offset tokens for each prompt. These tokens are fed into a two-way transformer with custom prompt tokens. The transformer’s output is divided into two streams: in the mask prediction stream, vertex tokens are concatenated with mask tokens. After passing through the FFN, these tokens divide the image embeddings into roof, building, and vertex masks. Using HiSup methods, the roof and vertex masks are combined to generate simplified polygonal roofs.

In the offset stream, offset tokens are processed by the FFNs in the ROAM structure, resulting in encoded offsets. These encoded offsets are then passed through the SOFA block, allowing them to adjust globally. The SOFA output is decoded using OBM’s methods, and the final polygonal footprints are derived by combining the polygonal roofs with the adjusted offsets.

3.3.2. Proposal Network

Promptable models commonly need help activating and promoting their functions. This was widely studied, especially in NLP (Gao et al., 2023). As a result, the proposal network was designed to prompt OBMv2 automatically. The network can be defined as an instance segmentation model, semantic segmentation model or object detection model. OBMv2 provides a bare semantic segmentation head inspired by Segmenter (Strudel et al., 2021) and SAM-HQ (Ke et al., 2024). Image embeddings from the image encoder will be passed to a segmenter mask transformer. The outputted image embeddings will be upsampled 4× as high-quality embeddings. These embeddings will be used to regress roofs. This paper applied more proposal modes to explore how to reach the maximum of OBMv2 in Sec.3.4.

3.3.3. Network Setting

The OBM’s losses were combined with two parts: prompt-level segmentation loss and offset losses in

ROAM, which can be expressed as:

$$\mathcal{L}_{OBM} = \mathcal{L}_{ROAM} + \mathcal{L}_{roof} + \mathcal{L}_{building} \quad (8)$$

where \mathcal{L}_{ROAM} is the loss of ROAM, and SmoothL1 Loss Girshick (2015) was applied for each offset head. \mathcal{L}_{roof} is CrossEntropy Loss Shannon (1948) of roof segmentation, and $\mathcal{L}_{building}$ is CrossEntropy Loss of building segmentation.

For two new tasks, CrossEntropy Loss is applied for roof semantic segmentation. The model outputs a vertex map for each building in prompt-level vertex segmentation. Because the vertex map contains the whole scope of the inputted image, this means most of the pixels will be valued as a negative sample by 0. Sparse positive key points will mislead the model to predict negative samples only. Via experiments, if the model uses a fixed window size to crop the building area, it can lead to severe grid effects. As a result, Dynamic Scope Binary Cross Entropy Loss (DS-BCE Loss) was designed for prompt-level vertex segmentation:

$$\mathcal{L}_{vertex} = \sum_{p \in Z + \Delta} -y_p \log y'_p - (1 - y_p) \log(1 - y'_p) \quad (9)$$

y_p and y'_p are pixels on ground truth and prediction maps at p . Z is the original prompted area, and Δ is a random small neighborhood of this area. Finally, OBMv2 was trained as:

$$\mathcal{L} = \lambda \times (\mathcal{L}_{OBM} + \beta \mathcal{L}_{vertex}) + \kappa \times \mathcal{L}_{seg} \quad (10)$$

λ and κ were parameters equal to 1 or 0 to control whether semantic heads would be trained together. β is a scale factor to balance the loss of vertex tasks and other tasks.

3.4. Extract building footprint with Multi-Information SyStem (MISS)

In the BFE problem, the multi-information can be divided into two aspects: integrating the given model with other building-related models to extract footprints, It is moreover, it extracts footprints with multiple results, including roof, building, and offsets. In terms of the prompting method, besides segmentation prompting, OBMv2 allows different types of prompting, including instance segmentation, object detection, *etc.* In experiments, semantic segmentation head result, LOFT (Wang et al., 2023a) results and Hybrid Task Cascade (HTC) (Chen et al., 2019)

instance segmentation were tested to provide prompts for OBMv2.

Another applicable knowledge from geography is that the information in the model overlaps each other. As shown in Fig.1, there are three features, roofs, the body of buildings and building offsets, can be extracted more easily than directly searching building footprints. Extracting footprints with roof segmentation and offsets is intuitive, and this method was popularly adopted in the aforementioned methods. In (c), the extracting method is also explicit: move the building mask along the roof-to-footprint offset, and the union between that and the building mask is the footprints. Similarly, if the building mask was moved in the opposite direction, the union would be the roof mask.

In (a), the situation was more complicated. The first step was to find a direction which could better represent the direction from roof to footprint. In this direction, a search algorithm was applied to detect the location of footprints by valuing different lengths of movement. Of course, we can also use the predicted global offset direction as this direction. In Algorithm 1, we introduced how to extract building footprint with only a roof and building segmentation. From

Algorithm 1 Footprint Searching

Require: Roof Segmentation: r_i , Building Segmentation: b_i , Iteration: N

Ensure: Related Footprint Segmentation: f_i

1: Angle list: $\alpha \leftarrow [0^\circ, 360^\circ]$

2: Unit Length of Offset: \bar{l}

3: Movements: $V = \begin{bmatrix} 1 & 0 & -\bar{l} \cos \alpha \\ 0 & 1 & -\bar{l} \sin \alpha \\ 0 & 0 & 1 \end{bmatrix}$

4: Moved Roofs: $\dot{R} = \{\dot{R}_1, \dot{R}_2, \dots, \dot{R}_{360}\} = V \cdot r_i$

5: Best Angle Value: $\theta = \arg \max_{j \in [0, 360]} S_j = \frac{\dot{R}_j \cap b_i}{r_i}$

6: Best Length Value:

$$l = \arg \min_{l_c} \left| \frac{\begin{bmatrix} 1 & 0 & -l_c \cos \theta \\ 0 & 1 & -l_c \sin \theta \\ 0 & 0 & 1 \end{bmatrix} \cdot r_i \cap b_i}{r_i} - 1 \right|$$

7: $f_i \leftarrow$ moving r_i via θ and l

lines 1-5, a linear search was applied to find a suitable moving angle for the roof to the footprint. Then, on this angle, binary searching was applied to determine

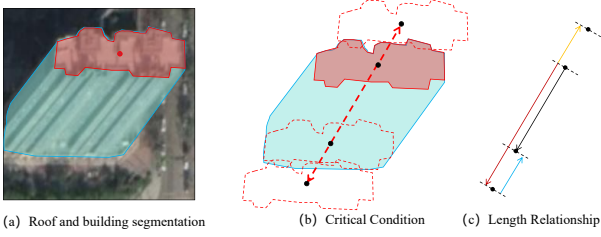


Figure 3: (a) describes the predicted roof and building for one building. (b) displays the critical condition of regressing building offset (c) abstracts the situation of (b).

the length of this moving path.

When applying spatial information in Algorithm 1 to extract footprints, The best Length Value was defined as the following critical condition in Fig.3.

Fig.3(c) illustrates how to extract a more accurate offset. The aforementioned binary search was applied twice for the **yellow offset** and **red offset**. As the length of **blue offset** equal to that of the **yellow offset**. The length of roof-to-building offset is equal to the **red offset** minor the **yellow offset**.

4. Experiment and Analysis

This section describes the data used in this work, justifies their choice, as well as specifies their sources. Then, the main results of the models are reported and analyzed. Lastly, a generalization test was conducted on the Huizhou test set.

4.1. Dataset

In our experiments, three datasets were employed to make a comparison:

(1)**BONAI** (Wang et al., 2023a): This dataset was launched with benchmark model LOFT. There are 3,000 train images and 300 test images, and the height and width of the images are 1024. The annotations for buildings include roof segmentation, footprint segmentation, offset, and height.

(2)**OmniCity-view3** (Li et al., 2022): OmniCity-view3 provided 17,092 train-val images and 4,929 test images in height and width 512. Footprint segmentation, building height, roof segmentation and roof-to-footprint offset were labelled for each building.

(3)**Huizhou test set** (Li et al., 2024a): This small dataset labelled images from a new city Huizhou, China. All buildings were plotted point-to-point by human annotators. The shape of the images is the same as BONAI, and there are over 7,000 buildings

included with offsets, roofs and footprint segmentations.

On the other hand, Li et al. (2024a) also newly inserted building segmentation task for aforementioned datasets by using roof segmentations and offsets.

4.2. Metrics

In this paper, models will be reported for both prompting mode and everything mode. Promptable models adopt metrics in OBM (Li et al., 2024a) and will provide mVL , mLL , mAL , aVL , aLL and aAL to evaluate offset prediction; and offset prediction in everything mode will be evaluated by a commonly used standard, End-point Error (EPE). For both modes, *precision*, *recall* and *f1score* are used to evaluate the final footprint prediction.

In this paper, we provide a new view of valuing models supporting both prompting and end-to-end extraction: different modes of the same model can be described as a "continuous entity". Prompting mode with accurate bounding boxes for all buildings performs as the ceiling of performance because prompting methods minimized the loss on region proposing. Meanwhile, different auto-prompting methods and different combinations of obtained information can be seen as discrete samples for this "continuous entity".

4.3. Experimental Settings

In the training process of our OBMv2 was trained in two stages. All images will be reshaped in 1024×1024 pixels. Experiments were conducted on a server with 4 NVIDIA RTX 3090. In the first stage, OBMv2 was trained in roof prompting mode. Then, proposal networks were trained solely. In the whole training progress, we used stochastic gradient descent (SGD) (Robbins and Monro, 1951) as the optimizer with batch size of 4 for 48 epochs, and initial step learning rate of 0.0025, a momentum of 0.9, and a weight decay of 10^{-4} . The number of parameters in OBMv2 is 77.69 M.

4.4. Main Result

In this section, we evaluate our methods on BONAI and OmniCity-view3. The main comparison will focus on LOFT (Wang et al., 2023a), Cascade LOFT and OBM between OBMv2 because these are models that are available for extensive experiments. In Tab.1, the displayed results were separated into three parts. The first part lists results from end-to-end

Table 1: Main results on BONAI (Wang et al., 2023a).

model	F1	Precision	Recall	EPE	mVL	mLL	mAL	aVL	aLL	aAL	R.IoU	R.BIoU
PANet	58.06	59.26	56.91	-	-	-	-	-	-	-	-	-
M RCNN	58.12	59.26	57.03	-	-	-	-	-	-	-	-	-
MTBR-Net	63.60	64.34	62.87	5.69	-	-	-	-	-	-	-	-
LOFT	64.42	64.43	64.41	4.85	-	-	-	-	-	-	-	-
Cas.LOFT*	62.58	63.67	61.52	4.79	-	-	-	-	-	-	-	-
MLS-BRN	66.36	65.90	66.83	4.76	-	-	-	-	-	-	-	-
p.LOFT	72.98	85.74	64.01	-	15.4	12.6	0.18	6.12	4.51	0.32	65.2	37.8
p.Cas.LOFT*	76.05	87.20	67.82	-	15.8	13.5	0.17	5.97	4.48	0.31	68.3	40.4
OBM	80.03	82.57	77.97	-	15.3	13.9	0.12	5.12	4.05	0.22	73.8	44.8
OBM [†]	78.65	80.41	77.21	-	17.0	15.7	0.12	5.38	4.35	0.22	76.5	47.9
Ours(mask)	78.74	79.85	77.91	-	17.0	15.8	0.11	5.46	4.40	0.22	77.7	50.0
Ours(poly.)	75.31	78.12	73.13	-	17.0	15.8	0.11	5.46	4.40	0.22	77.7	50.0

Note: * model is a model that we reproduce based on the author’s intention in paper (Wang et al., 2023a). OBM[†] was retrained in roof prompting mode. p. is short for *prompt*. Additionally, R.IoU and R.BIoU represent Roof IoU and Roof Boundary IoU. PANet (Liu et al., 2018) is an instance segmentation model named Path Aggregation Network. M RCNN represents Mask RCNN(He et al., 2017). MTBR-Net (Li et al., 2021) was published on ICCV2021. LOFT (Wang et al., 2023a) was published on TPAMI2023. MLS-BRN was published on CVPR2024. EPE, mVL, mLL, aVL and aLL were in pixels. Precision, Recall, F1, R.IoU and R.BIoU were measured in percentage(%).

models. In the second part, all available promptable models were compared with our proposed model in part three. From this table, we know that although OBMv2 can predict offset as accurately as that of OBM in terms of direction, it suffers from incorrect length prediction. This contributes to a clear drop in footprint flscore (approximately 1.29), and a similar drop in Precision and Recall can be found in this table. Roof mask quality was surprisingly improved compared with OBM despite the drop in footprint quality. The comparison and more analysis were provided in the discussion. For OBMv2, the footprint F1score decreased by 3.43 during the progress of vectorizing masks. This slight decline was commonly found in experiments because polygonal footprints commonly lost those complex edges for extracting simplified features.

To ensure SOFA block is applicable in all kinds of offset-based models, the results were listed in Tab.2. In this table, the same model in both prompting mode and roof prompting was written in the same line. SOFA block obviously brings gains for offset predic-

tion. *e.g.* SOFA reduced 0.33 and 0.36 pixels’ EPE for LOFT and Cascade LOFT. mVL reduced by 0.8 pixels for prompt LOFT.

Experiments on OmniCity-view3 further demonstrate the advance of our OBMv2. In this table, OBMv2 nearly outperformed all mentioned models. Although vectorized footprint polygons still have lower

Table 3: Experimental results on OmniCity-view3.

model	F1	Precision	Recall	EPE	mVL	mLL	mAL	aVL	aLL	aAL
M RCNN	69.75	69.74	69.76	-	-	-	-	-	-	-
LOFT	70.46	68.77	72.23	6.08	-	-	-	-	-	-
MLS-BRN	72.25	69.57	75.14	5.38	-	-	-	-	-	-
p.LOFT	82.27	90.63	75.81	-	54.3	48.5	0.65	7.57	5.29	0.70
p.Cas.LOFT	83.75	91.62	77.54	-	52.9	48.4	0.62	7.25	5.12	0.69
OBM	86.03	90.17	82.52	-	56.9	53.7	0.66	6.69	5.15	0.64
Ours(mask)	88.42	90.06	87.01	-	51.5	47.9	0.63	6.15	4.65	0.59
Ours(poly.)	87.61	90.76	84.93	-	51.5	47.9	0.63	6.15	4.65	0.59

F1score compared with its mask footprints, OBMv2 outperformed all mentioned models. In OBMv2, polygonal results even have better Precision compared with mask results(+0.7). Moreover, OBMv2 performed better than any other models in terms of offset prediction. aVL of OBMv2 is 1.423 pixels lower than that of prompt LOFT, and 0.544 pixels lower than figure for OBM. Comparing model performance, we found that the performance of OBMv2 on two distinct datasets was different.

In Fig.4, visualized results in the prompt mode were provided. The first and second lines of illustrations were selected from BONAI(Wang et al., 2023a). The third and fourth lines were from OmniCity-view3(Li et al., 2022), and the last line was from Huizhou(Li

Table 2: SOFA block ablation studies on BONAI.

model	EPE	mVL	mLL	mAL	aVL	aLL	aAL
LOFT	4.85	15.4	12.6	0.18	6.12	4.51	0.32
LOFT+SOFA	4.52	14.6	12.6	0.13	5.62	4.49	0.22
Cas.LOFT	4.79	15.8	13.5	0.17	5.97	4.48	0.31
Cas.LOFT+SOFA	4.43	15.3	13.4	0.12	5.64	4.44	0.22
OBM	-	15.3	13.9	0.12	5.12	4.05	0.22
OBM+SOFA	-	15.3	13.9	0.11	5.08	4.04	0.21
OBM [†]	-	17.0	15.7	0.12	5.38	4.35	0.22
OBM [†] +SOFA	-	16.8	15.7	0.11	5.36	4.35	0.21

et al., 2024a). Our model can provide polygonal results, which are more editable compared with other models.

A generalization test was conducted at the Huizhou test set. All models were pre-trained on BONAI, and there was no extra training. In predicting footprints,

Table 4: Experimental results on Huizhou test set.

model	F1	Precision	Recall	aVL	aLL	aAL
p.LOFT	72.56	83.02	65.33	7.935	6.449	0.752
p.Cas.LOFT	75.83	81.71	71.13	7.894	5.938	0.818
OBM	81.53	78.80	84.80	4.898	4.351	0.169
OBM [†]	80.30	79.04	81.85	4.985	4.412	0.198
Ours(mask)	80.36	78.99	82.18	4.959	4.636	0.144
Ours(poly.)	75.35	77.04	74.25			

results of OBM and OBMv2 exhibit similar attributes with them on BONAI, *e.g.* the gap between f1scores of footprints predicted by OBMv2 on BONAI(75.31) and Huizhou Test(75.35) is 0.04.

In summary, OBMv2 can directly predict footprint polygons, the performance of which showcased a certain generalization ability. In some datasets, OBMv2 can even partially outperform the aforementioned models with polygonal results. The newly proposed SOFA structure can be widely applied in different models and bring gains for offset prediction.

4.5. Multi-information for BEF problem

Multi-information can be divided into two classes: information extracted by different kinds of building related models and extracted multi-information by OBMv2. Human-plotted prompts will motivate models to reach their ceiling performance. In this part, footprints f1score were selected to measure mask ability; meanwhile, EPE and aVL, which are similar in definition, were used to measure offset ability. Each model will be scattered on coordinates. To facilitate comparison, BONAI was used due to its diverse open-source methods and known experimental results.

In Fig.5, the BEF problem was solved with different information. For promptable models, OBM and OBMv2, building segmentation with offsets can predict better building footprint(F1score +1.37 and +0.23 respectively). End-to-end ROI-based can also extract footprint with building segmentation and offsets, which provides similar performance with related models using roof and offset. Additionally, extracting footprints with roof and building segmentation has been proved applicable, although offsets regressed in this version were inaccurate compared with models using roofs. All models can provide better results than Mask RCNN.

The automatic extraction of building footprints commonly relies on proposal regions. In Tab.5, OBMv2 was tested with different region proposal functions. Additionally, utilizing different sources of information to extract footprint print was also examined.

Table 5: Auto extraction results on BONAI test set.

model	F1	Precision	Recall	EPE
M RCNN	56.12	57.02	55.26	-
LOFT(r.o.)	64.42	64.43	64.41	4.85
LOFT(b.o.)	61.97	61.41	62.55	5.83
Cas.LOFT(r.o.)	62.58	63.67	61.52	4.79
Cas.LOFT(b.o.)	61.67	64.59	59.00	5.23
MLS-BRN	66.36	65.90	66.83	4.76
Ours+HTC(r.o.)	61.48	55.19	74.79	4.59
Ours+HTC(b.o.)	61.48	55.13	74.99	
Ours+seg.	55.20	64.66	50.47	-

r., b., o. and d. represent roof mask, building mask, offset and offset direction.

With the help of HTC, OBMv2 can automatically extract building footprints, and the Recall of this model is higher (+8.16) than the former SOTA MLS-BRN. By adjusting different prompting modes, OBMv2 can also reach a similar Precision of MLS-BRN (-1.24).

In Fig.6, footprints extracted by auto mode were compared with each other. Our model can still provide polygonal results compared with other models.

5. Ablation

This section will examine the proposed algorithms and blocks. Apart from the SOFA block, the aforementioned algorithms proposed for extracting footprints with different information also need ablation.

5.1. Ablation of SOFA block

Unlike other transformer blocks, SOFA block was developed not sensitive to the input length of embedded tokens. Because of this feature, SOFA block can adapt to any offset-based models. SOFA block was trained in the last stage after all other blocks finished training. In Tab.2, SOFA block was applied in all open-source models and can reduce both prompt-level and instance-level offset errors. *e.g.* EPE of LOFT on the BONAI dataset declined by 0.33 pixels.

5.2. Multi-information

To ensure the proposed algorithms can extract building footprints, ablation studies were conducted with ground truth labels.

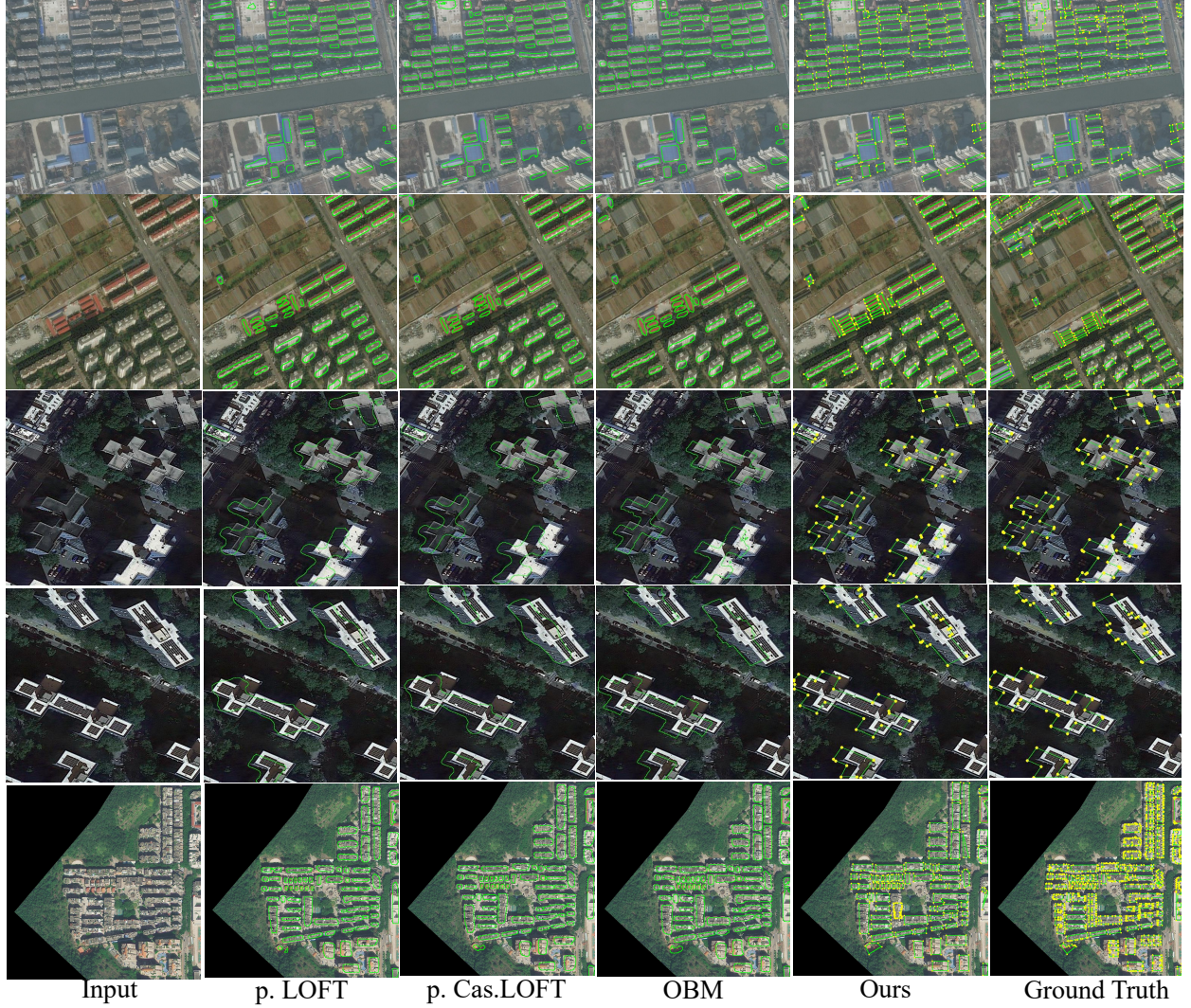


Figure 4: Main results extracted by prompting mode. The green lines represent predicted building footprint boundaries, and the yellow points are key nodes of the building.

Table 6: Extract footprints with different ground truth labels on BONAI test set.

Model	F1	Precision	Recall	aVL
b.+o.	98.22	98.60	97.88	0
r.+o.	98.55	99.30	97.84	0
b.+r.	87.87	88.67	87.11	5.83
b.+r.+d.	94.37	98.17	91.69	0.67

r., b., o. and d. represent roof mask, building mask, offset and offset direction.

From Tab.6, our proposed algorithms can accurately extract building footprints via different information. Although our algorithms can extract footprints merely with roof and building segmentations, grid-based digital images are always limited by image continuity. The influence of this problem is more severe, especially on the representations of buildings with short offsets, *e.g.* an offset with length 1 pixel,

there are only 4 points nearby that can represent its endpoint. This ambiguity leads to a poor perception of direction. As a result, when the offset direction was given, the *aVL* dropped by 5.16 pixels and the f1-score of footprints increased by 6.5%.

5.3. Proposal Methods

OBMv2 can receive almost all kinds of models which can provide bounding boxes related to buildings. Except for an extra segmentation head on OBMv2, OBMv2 was integrated with other models that can provide roof-bounding boxes or segmentations. These outputs perform as rough extraction results and OBMv2 will correct and refine them.

In Tab.7, OBMv2 was integrated with its segmentation head, HTC and LOFT. Specifically, HTC and

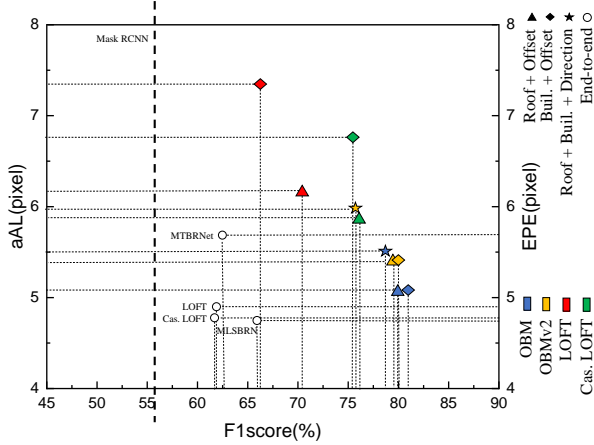


Figure 5: Extracting footprints with multi-types of information.

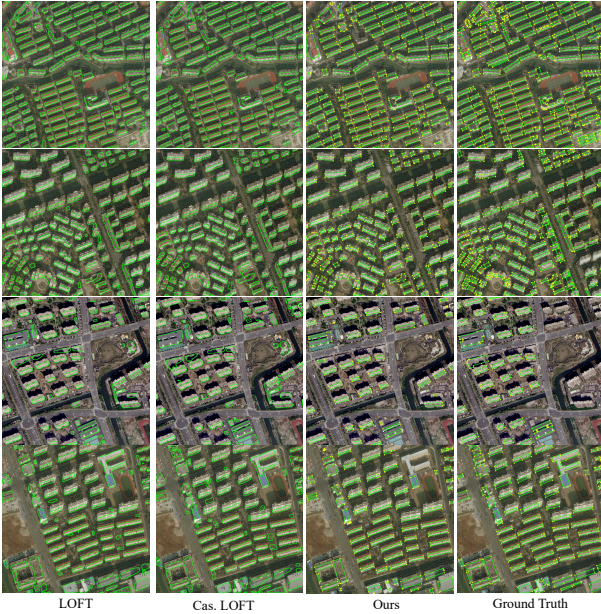


Figure 6: Main results extracted by prompting mode

Table 7: Extract footprints with other roof extraction models on BONAI test set.

Model	F1	Precision	Recall	EPE
OBMv2	78.74	79.85	77.91	-
+eve	59.67	68.06	55.32	5.03
+HTC♥	61.48	55.19	74.80	4.59
+HTC♠	51.79	39.23	85.29	4.92
+HTC♣	60.70	59.18	66.32	4.42
+LOFT♠	56.24	44.01	84.33	5.07
+LOFT♣	60.26	56.32	68.48	4.59

LOFT are matched with different NMS strategies. ♠ represents soft NMS algorithms with a score threshold of 0.05, IoU threshold of 0.5, and maximum of 2000 instances per image. ♣ represents NMS algorithms with a score threshold of 0.1, IoU threshold of 0.5, and a maximum of 2000 instances per image. ♥ leverages result from ♠, but the same instance, which

was repeatedly predicted, will be merged as one instance.

Soft NMS algorithm gives almost all bounding boxes with a very low score threshold. This means most output boxes will be selected as final outputs. Consequently, they can provide results with high Recall, but OBMv2 was trained with annotations that can cover the whole building or roof. As a result, the Precision was not good. *e.g.* Precision of OBMv2 + HTC♠ is lower than that of OBMv2 + HTC♥ by 15.96%, although the Recall of OBMv2 + HTC♠ is higher than that of OBMv2 + HTC♥ by 10.49%. Finally, the score of OBMv2 + HTC♠ was adversely influenced, which only reached 51.79%.

6. Discussion

6.1. Try to understand SOFA

As shown in 7, SOFA block is trainable with one single learnable parameter w . This parameter was finally set to 0.

Let us try to understand this figure. During self-offset attention, w performs as a global weight for relatively longer offsets. Before the operation of softmax, all weighted $(\rho - \rho_i)^2$ will be equal to 0, and then the softmax function will weight each \vec{u}_i equally to determine the final output.

When w was set to trainable in experiments, its value fluctuated around 0.0452. This figure almost equals 0, and the data flow follows the explanation above. The result may imply that manually designed features generated by measuring lengths of offsets are not the best method to optimize offsets. In the future, SOFA attention may be upgraded by replacing coordinate projection with other learnable embedding progress.

6.2. External models and multi-solutions of BFE

The use of external prompts for interactive models has been studied in many cases. *e.g.* contrastive Language-Image Pre-training (CLIP) was trained on over 400 million pairs of images and text (Radford et al., 2021). When researchers conduct experiments on classifying ImageNet (Deng et al., 2009). The researchers found that using a prompt template "A photo of a {label}" can directly improve the accuracy by 1. 3% compared to using a single category word "{label}". In the video recognition zone, FineCLIPER (Chen et al., 2024a) using regenerated video captions for facial activities also improves the quality of the

model. In the BFE problem, Li et al. (2024a) discovered that slightly larger building prompts can extract better footprints than fully fitting box prompts. Another example is the application of the Large Language Model (LLM). RAG in LLM was another key tool to improve the final generated results (Lewis et al., 2020). *e.g.* Query2doc (Wang et al., 2023b) use pseudo-documents prompting and concatenates them with the original query to improve predicting quality.

BFE problems solved by a promptable model like OBMv2 must also consider similar problems. Researchers who proposed OBM, the former version of OBMv2, found that slightly inaccurate prompts can improve the performance of the model (Li et al. (2024a)). In this paper, OBMv2 extended the "Prompting Test" to external models and studied three kinds of methods to extract footprints.

Except Fig.5 and Tab.7, more interesting methods must help the model reach and exceed "the ceiling performance of using Ground Truth prompts".

6.3. Limitations of OBMv2

Limitations of OBMv2 are mainly generated in two streams: the limited interactive visual zone and the training methods. The roof prompted OBM2. The roof prompts make the attention of OBMv2 excessively focused on the "building top" zone. Thus, multi-attention is less likely to notice the features in other parts of a building, although a two-way transformer helps OBMv2 reference features from other buildings.

On the other hand, OBMv2 was trained with noised ground truth boxes, which can cover all the pixels of each roof. However, the bounding boxes received by OBMv2 tend to cover only a small pitch of one building when integrated with other models, as shown in Fig.7. For such box prompts, OBMv2 cannot predict accurate offsets. Then, the corresponding roofs were consequently moved to the wrong places because of uncertainty. That is why in Tab.7, soft NMS has high recall but low precision.

6.4. The benefit of building task

Considering building-related information was one of the contributions of this paper. For OBM and OBMv2, using building segmentation and offset robustly improves the quality of extracted footprints. We carefully analyzed the results of the predicted roof and building segmentation to find an explanation. We found that the edge of a roof and building

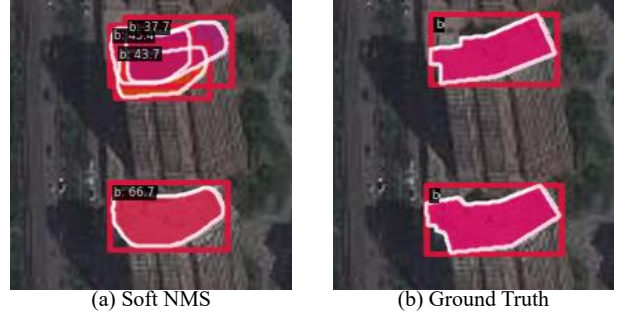


Figure 7: Some mistake samples of roof extraction made by HTC and Ground Truth label

facade is not that obvious compared with the edge between the building and background in one remote sensing image.

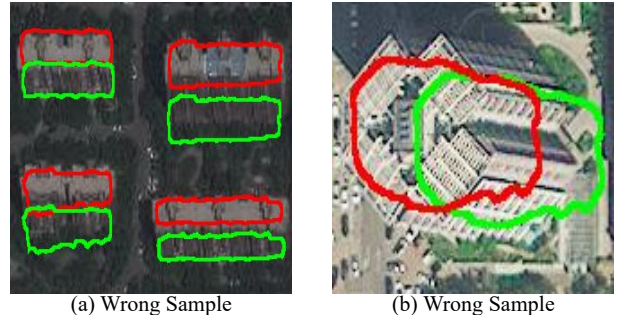


Figure 8: Some mistake samples of roof extraction

Fig.8 shows some typical samples that predict false roofs due to the "edge problem". Low roof quality but relatively correct offsets finally lead to a poor quality footprint. The situation mentioned above can be improved by using building segmentation as in Fig.1(c).

6.5. Why does OBMv2 not always outperform other models?

OBMv2 is not always better than other models. *e.g.* On BONAI (Wang et al., 2023a), OBMv2 partially outperforms OBM in Tab.1, but experiments on OmniCity (Li et al., 2022) showcase the ability of OBMv2. From Fig.4, we speculate that this is likely due to the different pixel proportions occupied by buildings in the same image. The image embeddings from the ViT encoder are downsampled by $16\times$. This downsampling process will adversely influence the quality of embeddings, especially when objects in

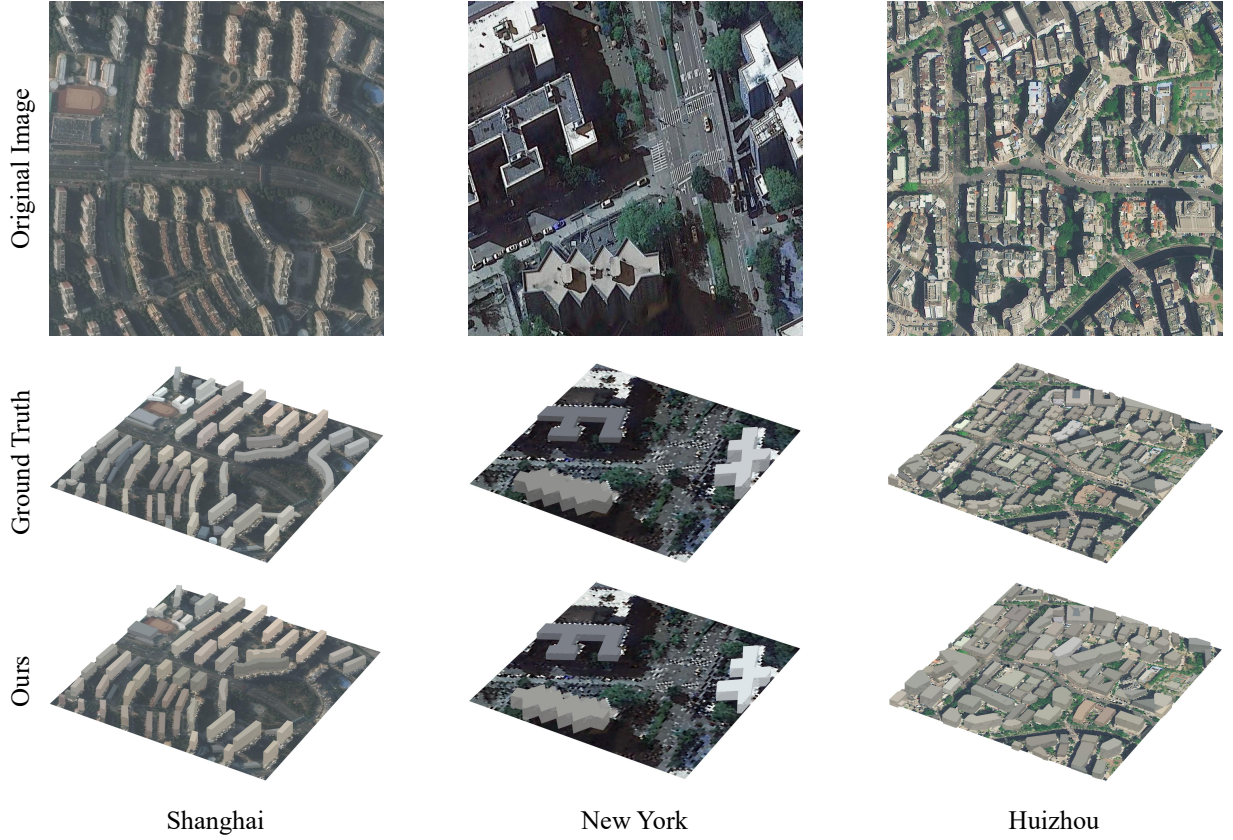


Figure 9: Monocular 3D building reconstruction results from polygonal outputs of OBMv2

images only occupy a small number of pixels. Unfortunately, this feature is very obvious on BONAI compared to OmniCity. BONAI data are downsampled by $16\times$, while this information loss of OmniCity only is only $4\times$. In other words, multiscale prediction may perform as a powerful tool in augmentation.

6.6. Polygonal results for 3D building reconstruction with monocular images

3D building reconstruction is another meaningful topic which was popularly mentioned by Li et al. (2021, 2024c,b). As illustrated in Fig.9, OBMv2 can also provide similar results using the concept "relative height map" proposed by Li et al. (2024a). Since our model can directly output vectorized building layouts, the OBMv2 results present more sharply defined edges in the visual representation of buildings.

However, the challenge, as the last line in Fig.4, of OBMv2, is the poor performance of detecting key points when performing the generalization test. An incomplete inflexion point prediction significantly affects polygonal results, which is also risky for 3D reconstruction tasks based on this type of method. For

this, we may go deeper with the proposed methods Wang et al. (2024) to study how to get better polygonal results.

The introduction of the offset token holds great significance in the current era of large models. For instance, as the accuracy of urban segmentation improves, the offset token will contribute to the simulation of urban 3D environments under monocular vision. Moreover, the technique of tokenizing offsets will promote the integration of urban-related information with various large models in the remote sensing field, such as GeoChat(?), which will lead to the creation of more meaningful works.

6.7. Future work

Although OBM and OBMv2 outperform other end-to-end models in prompt mode, their automatic mode still cannot touch their ceiling performance. Future exploration may focus on how to tap into the model's potential, such as RAG in LLM. On the other hand, except for BONAI(Wang et al., 2023a) and OmniCity(Li et al., 2022), there is little valid data to fine-tune models. However, many of the currently de-

veloped models need a vast amount of data to train or fine-tune. As a result, we advocate more teams to democratize their data. By sharing and making data more accessible, we can collectively make significant strides in the field of the BFE problem, and this should be a key focus for all of us in the field.

7. Conclusion

This paper provides a model which can extract polygonal building footprints automatically and interactively. For its vertex computing property, OBMv2 can directly extract building footprints. Inside the model, Self Offset Attention (SOFA) was designed to correct short offsets in our model for the typical pattern of predicting roof-to-footprint offset. Then, this paper discussed using multiple pieces of information to predict footprints and better integrate them with other models to extract building footprints automatically. Additionally, BFE problems can be solved from different perspectives, and using building segmentation and offset can cleverly avoid the problem of unclear edges between the roof and facade. The OBM series models are significantly better than other models in prompt mode, with OBMv2 and OBM showing their respective advantages on the datasets used in the experiment.

References

- Chen, H., Huang, H., Dong, J., Zheng, M., Shao, D., 2024a. Finecliper: Multi-modal fine-grained clip for dynamic facial expression recognition with adapters. arXiv preprint arXiv:2407.02157.
- Chen, H., Huang, Y., Huang, H., Ge, X., Shao, D., 2024b. Gaussianvton: 3d human virtual try-on via multi-stage gaussian splatting editing with image prompting. arXiv preprint arXiv:2405.07472.
- Chen, K., Pang, J., Wang, J., Xiong, Y., Li, X., Sun, S., Feng, W., Liu, Z., Shi, J., Ouyang, W., Loy, C. C., Lin, D., 2019. Hybrid task cascade for instance segmentation. In: IEEE Conf. Comput. Vis. Pattern Recog.
- Christie, G., Abujder, R. R. R. M., Foster, K., Hagstrom, S., Hager, G. D., Brown, M. Z., 2020. Learning geocentric object pose in oblique monocular images. In: Proceedings of the IEEE/CVF Conference on Computer Vision and Pattern Recognition. pp. 14512–14520.
- Deng, J., Dong, W., Socher, R., Li, L.-J., Li, K., Fei-Fei, L., 2009. Imagenet: A large-scale hierarchical image database. In: IEEE Conf. Comput. Vis. Pattern Recog. pp. 248–255.
- Douglas, D. H., Peucker, T. K., 1973. Algorithms for the reduction of the number of points required to represent a digitized line or its caricature. *Cartographica: the international journal for geographic information and geovisualization* 10 (2), 112–122.
- Gao, Y., Xiong, Y., Gao, X., Jia, K., Pan, J., Bi, Y., Dai, Y., Sun, J., Wang, H., 2023. Retrieval-augmented generation for large language models: A survey. arXiv preprint arXiv:2312.10997.
- Girard, N., Smirnov, D., Solomon, J., Tarabalka, Y., 2021. Polygonal building extraction by frame field learning. In: 2021 IEEE/CVF Conference on Computer Vision and Pattern Recognition (CVPR). pp. 5887–5896.
- Girshick, R., 2015. Fast r-cnn. In: Int. Conf. Comput. Vis. pp. 1440–1448.
- Guo, G., Shao, D., Zhu, C., Meng, S., Wang, X., Gao, S., 2024. P2p: Transforming from point supervision to explicit visual prompt for object detection and segmentation. *IJCAI*.
- He, K., Gkioxari, G., Dollár, P., Girshick, R., 2017. Mask R-CNN. In: Int. Conf. Comput. Vis. pp. 2980–2988.
- Inglada, J., 2007. Automatic recognition of man-made objects in high resolution optical remote sensing images by SVM classification of geometric image features. *ISPRS J. Photogramm. Remote Sens.* 62 (3), 236–248.
- Ke, L., Ye, M., Danelljan, M., Tai, Y.-W., Tang, C.-K., Yu, F., et al., 2024. Segment anything in high quality. *Adv. Neural Inform. Process. Syst.* 36.
- Khattak, S. R., Buckstein, D. S., Hogue, A., 2013. Reconstructing 3d buildings from lidar using level set methods. In: 2013 International Conference on Computer and Robot Vision. pp. 151–158.
- Kirillov, A., Mintun, E., Ravi, N., Mao, H., Rolland, C., Gustafson, L., Xiao, T., Whitehead, S., Berg, A. C., Lo, W.-Y., et al., 2023. Segment anything. In: Int. Conf. Comput. Vis. pp. 4015–4026.
- Kunwar, S., Chen, H., Lin, M., Zhang, H., D’Angelo, P., Cerra, D., Azimi, S. M., Brown, M., Hager, G., Yokoya, N., Hänsch, R., Le Saux, B., 2021. Large-scale semantic 3-d reconstruction: Outcome of the 2019 ieee grss data fusion contest—part a. *IEEE Journal of Selected Topics in Applied Earth Observations and Remote Sensing* 14, 922–935.
- Lafarge, F., Descombes, X., Zerubia, J., Pierrot-Deseilligny, M., 2010. Structural approach for building reconstruction from a single DSM. *IEEE Trans. Pattern Anal. Mach. Intell.* 32 (1), 135–147.
- Lewis, P., Perez, E., Piktus, A., Petroni, F., Karpukhin, V., Goyal, N., Küttler, H., Lewis, M., Yih, W.-t., Rocktäschel, T., Riedel, S., Kiela, D., 2020. Retrieval-augmented generation for knowledge-intensive nlp tasks. In: Larochelle, H., Ranzato, M., Hadsell, R., Balcan, M., Lin, H. (Eds.), *Advances in Neural Information Processing Systems*. Vol. 33. Curran Associates, Inc., pp. 9459–9474.
- Li, K., Deng, Y., Kong, Y., Liu, D., Chen, J., Meng, Y., Ma, J., 2024a. Prompt-driven building footprint extraction in aerial images with offset-building model. URL <https://arxiv.org/abs/2310.16717>
- Li, W., Hu, Z., Meng, L., Wang, J., Zheng, J., Dong, R., He, C., Xia, G.-S., Fu, H., Lin, D., 2024b. Weakly supervised 3-d building reconstruction from monocular remote sensing images. *IEEE Trans. Geosci. Remote Sens.* 62, 1–15.
- Li, W., Lai, Y., Xu, L., Xiangli, Y., Yu, J., He, C., Xia, G.-S., Lin, D., 2022. Omnicity: Omnipotent city understanding with multi-level and multi-view images. arXiv e-prints, arXiv-2208.
- Li, W., Meng, L., Wang, J., He, C., Xia, G.-S., Lin, D., 2021. 3d building reconstruction from monocular remote sensing images. In: Int. Conf. Comput. Vis. pp. 12548–12557.

- Li, W., Yang, H., Hu, Z., Zheng, J., Xia, G.-S., He, C., 2024c. 3d building reconstruction from monocular remote sensing images with multi-level supervisions. arXiv preprint arXiv:2404.04823.
- Lian, Y., Feng, T., Zhou, J., Jia, M., Li, A., Wu, Z., Jiao, L., Brown, M., Hager, G., Yokoya, N., Hänsch, R., Saux, B. L., 2021. Large-scale semantic 3-d reconstruction: Outcome of the 2019 ieee grss data fusion contest—part b. *IEEE J. Sel. Topics Appl. Earth Observations Remote Sens.* 14, 1158–1170.
- Liu, S., Qi, L., Qin, H., Shi, J., Jia, J., June 2018. Path aggregation network for instance segmentation. In: *IEEE Conf. Comput. Vis. Pattern Recog.*
- Nadaraya, E. A., 1964. On estimating regression. *Theory Probab. Its Appl.* 9 (1), 141–142.
- Ortner, M., Descombes, X., Zerubia, J., 2008. A Marked Point Process of Rectangles and Segments for Automatic Analysis of Digital Elevation Models. *IEEE Trans. Pattern Anal. Mach. Intell.* 30 (1), 105–119.
- Priestnall, G., Jaafar, J., Duncan, A., 2000. Extracting urban features from lidar digital surface models. *Computers, Environment and Urban Systems* 24 (2), 65–78.
- Radford, A., Kim, J. W., Hallacy, C., Ramesh, A., Goh, G., Agarwal, S., Sastry, G., Askell, A., Mishkin, P., Clark, J., Krueger, G., Sutskever, I., 18–24 Jul 2021. Learning transferable visual models from natural language supervision. In: Meila, M., Zhang, T. (Eds.), *Int. Conf. Mach. Learn. Vol. 139 of Proc. of Mach. Learn. Res. PMLR*, pp. 8748–8763. URL <https://proceedings.mlr.press/v139/radford21a.html>
- Ravi, N., Gabeur, V., Hu, Y.-T., Hu, R., Ryali, C., Ma, T., Khedr, H., Rädle, R., Rolland, C., Gustafson, L., et al., 2024. Sam 2: Segment anything in images and videos. arXiv preprint arXiv:2408.00714.
- Robbins, H., Monro, S., 1951. A stochastic approximation method. *The annals of mathematical statistics*, 400–407.
- Shannon, C. E., 1948. A mathematical theory of communication. *Bell Syst. Tech. J.* 27 (3), 379–423.
- Strudel, R., Garcia, R., Laptev, I., Schmid, C., October 2021. Segmenter: Transformer for semantic segmentation. In: *Int. Conf. Comput. Vis.* pp. 7262–7272.
- Vaswani, A., Shazeer, N., Parmar, N., Uszkoreit, J., Jones, L., Gomez, A. N., Kaiser, L. u., Polosukhin, I., 2017. Attention is all you need. In: Guyon, I., Luxburg, U. V., Bengio, S., Wallach, H., Fergus, R., Vishwanathan, S., Garnett, R. (Eds.), *Adv. Neural Inform. Process. Syst. Vol. 30. Curran Associates, Inc.*
- Viola, P., Jones, M., 2001. Rapid object detection using a boosted cascade of simple features. In: *IEEE Conf. Comput. Vis. Pattern Recog. Vol. 1.* pp. I–I.
- Wang, C., Chen, J., Meng, Y., Deng, Y., Li, K., Kong, Y., 2024. Sampolybuild: Adapting the segment anything model for polygonal building extraction. *ISPRS J. Photogramm. Remote Sens.* 218, 707–720. URL <https://www.sciencedirect.com/science/article/pii/S0924271624003563>
- Wang, J., Meng, L., Li, W., Yang, W., Yu, L., Xia, G.-S., 2023a. Learning to Extract Building Footprints From Off-Nadir Aerial Images. *IEEE Trans. Pattern Anal. Mach. Intell.* 45 (1), 1294–1301.
- Wang, L., Yang, N., Wei, F., 2023b. Query2doc: Query expansion with large language models. In: *Conf. Empirical Methods Natural Lang. Process.*
- URL <https://openreview.net/forum?id=QH4EMvwF8I>
- Watson, G. S., 1964. Smooth regression analysis. *Sankhyā: The Indian Journal of Statistics, Series A*, 359–372.
- Wei, S., Ji, S., Lu, M., 2019. Toward automatic building footprint delineation from aerial images using cnn and regularization. *IEEE Trans. Geosci. Remote Sens.* 58 (3), 2178–2189.
- Xu, B., Xu, J., Xue, N., Xia, G.-S., 2023. Hisup: Accurate polygonal mapping of buildings in satellite imagery with hierarchical supervision. *ISPRS J. Photogramm. Remote Sens.* 198, 284–296.
- Zhu, A.-X., Lu, G., Liu, J., Qin, C.-Z., Zhou, C., 2018. Spatial prediction based on third law of geography. *Annals of GIS* 24 (4), 225–240.
- Zorzi, S., Bittner, K., Fraundorfer, F., 2021. Machine-learned regularization and polygonization of building segmentation masks. In: *Int. Conf. Pattern Recog. IEEE*, pp. 3098–3105.